Catalysis Today 185 (2012) 263–269

Contents lists available at ScienceDirect

Catalysis Today

journal homepage: www.elsevier.com/locate/cattod

Photocatalytic conversion of carbon dioxide into methanol using optimized layered double hydroxide catalysts

Naveed Ahmed [a], Motoharu Morikawa [b], Yasuo Izumi [a,*]

[a] Department of Chemistry, Graduate School of Science, Chiba University, Yayoi 1-33, Inage-ku, Chiba 263-8522, Japan
[b] Department of Nanomaterial Science, Graduate School of Advanced Integration Science, Chiba University, Yayoi 1-33, Inage-ku, Chiba 263-8522, Japan

ARTICLE INFO

Article history:
Received 31 May 2011
Received in revised form 1 August 2011
Accepted 9 August 2011
Available online 1 September 2011

Keywords:
CO_2
Photoreduction
Methanol
Layered double hydroxide
Interlayer copper

ABSTRACT

The photocatalytic reduction of carbon dioxide into methanol was enabled between the Zn–Ga or Zn–Cu–Ga hydroxide layers using hydrogen and was promoted by the partial desorption of structural water stuffed between the cationic layers. The photoreduction rate obtained using $[Zn_{1.5}Cu_{1.5}Ga(OH)_8]^+{}_2(CO_3)^{2-}\cdot mH_2O$ was improved by replacing interlayer carbonate anions with $[Cu(OH)_4]^{2-}$ to 0.49 $\mu mol_{Methanol}\ h^{-1}\ g_{cat}{}^{-1}$, and the methanol selectivity was 88 mol%. At the molar level, interlayer Cu species was 5.9 times more active than the octahedral Cu sites in the cationic layers. The bandgap value was evaluated as 3.0 eV for the semiconductor $[Zn_{1.5}Cu_{1.5}Ga(OH)_8]^+{}_2[Cu(OH)_4]^{2-}\cdot mH_2O$. Direct electronic transition from O 2p to metal 3d, 4s, or 4p was responsible for the photocatalysis excited largely by ultraviolet (UV), and to a lesser extent by visible light.

1. Introduction

There has been growing interest in the development of novel artificial methods that capture and concentrate large quantities of atmospheric carbon dioxide for subsequent conversion into fuels. Use of these methods is considered to have the potential to help alleviate major environmental problems relating to global warming and the scarcity of sustainable and secure energy sources [1,2]. Employing similarities that exist with the reaction of light during photosynthesis in green plants, phytoplankton, and algae, many researchers [3–5] have tried to attempt the photoreduction of CO_2 coupled with water. However, due to thermodynamic limitations, the conversion of CO_2 into fuels (such as methanol and formic acid) is extremely unfavorable [6]. In contrast, the conversion of CO_2 and hydrogen into fuel shows promise for application in the near future if H_2 can be obtained from water using sunlight.

Recently, the photoreduction of CO_2 and H_2 into methanol was reported for the first time using semiconductor layered double hydroxide (LDH) photocatalysts that were formulated as $[Zn^{II}{}_{1-x-y}Cu^{II}{}_yM^{III}{}_x(OH)_2]^{x+}{}_{2/x}(CO_3)^{2-}\cdot mH_2O$ (M = Ga, Al; $0 \le x \le 1/3$; $0 \le y \le 1/2$; $m \sim 1/x$) [6]. The methanol selectivity (26 mol%) obtained using Zn–Cu–Al LDH catalysts was improved to 68 mol% using Zn–Cu–Ga LDH catalysts. For practical applications, the catalytic rates of CO_2 photoreduction are essential. Overall photocatalytic rates (250 $nmol\ h^{-1}\ g_{cat}{}^{-1}$) obtained using Zn–Cu–Ga catalysts [6] need to be accelerated by the optimization of their electronic state, concentrating the number of active sites, and the design of their interlayer reaction space.

In the interlayer space of LDH photocatalysts, CO_2 was suggested for the reaction with the hydroxy group bound to the Cu sites to form a hydrogen carbonate intermediate [6]. Under UV–visible light, the Cu ions in the cationic layer facilitated charge separation utilizing the reduction-oxidation (redox) of $Cu^{II} \rightleftarrows Cu^{I}$. Hydrogen carbonate species were gradually reduced to formic acid, formaldehyde, and finally to methanol utilizing the trapped photogenerated electrons as Cu^{I} ions [6]. Therefore, the interlayer space of these LDH photocatalysts served as an active pocket for the reduction of CO_2 to methanol. An increase in the available reaction space would lead to enhanced photocatalytic activity.

The shape and size controls of ordered one dimensional nano/mesopores of metal oxides [7] and ordered two dimensional spaces between clay layers [8] were reported to lead to improved catalysis. The LDH compounds are advantageous in that they increase the available reaction space between cationic layers by the desorption of structural water molecules and carbonate anions while maintaining the regular stacked layer structure at 423–473 K [9,10]. As the quantity of Cu^{II} sites in the cationic layers increased, the photocatalytic formation rates of methanol were enhanced [6]. If photoactive Cu sites can also be accommodated as anion species of LDHs between the cationic layers, the photocatalytic rates per unit amount of catalyst would be further optimized.

* Corresponding author. Tel.: +81 43 290 3696; fax: +81 43 290 2783.
E-mail address: yizumi@faculty.chiba-u.jp (Y. Izumi).

0920-5861/$ – see front matter © 2011 Elsevier B.V. All rights reserved.
doi:10.1016/j.cattod.2011.08.010

In this study, the available interlayer reaction space was increased by the pretreatment of LDH catalysts. Also $[Cu(OH)_4]^{2-}$ anion species was introduced between the cationic layers of LDHs. The effects of these modifications on the structure, physical properties, and photocatalytic performance were studied. In addition, we demonstrated the feasibility of CO_2 reduction coupled with water.

2. Methods

2.1. Catalyst syntheses

$[Zn_3Ga(OH)_8]^+_2(CO_3)^{2-}\cdot mH_2O$ and $[Zn_{1.5}Cu_{1.5}Ga(OH)_8]^+_2(CO_3)^{2-}\cdot mH_2O$ LDH compounds were synthesized using a reported procedure [6]. They are abbreviated as $Zn_3Ga|CO_3$ and $Zn_{1.5}Cu_{1.5}Ga|CO_3$, respectively. Corresponding LDH samples consisting of anionic copper species between the $[Zn_3Ga(OH)_8]^+$ or $[Zn_{1.5}Cu_{1.5}Ga(OH)_8]^+$ cationic layers were synthesized following a similar procedure, in order to use $(NH_4)_2CuCl_4\cdot 2H_2O$ as the source of $[CuCl_4]^{2-}$ anions.

For the synthesis of $[Zn_3Ga(OH)_8]^+$ LDH consisted of anionic Cu species, 20 mL solution consisting of both 0.75 M $Zn(NO_3)_2\cdot 6H_2O$ and 0.25 M $Ga(NO_3)_3\cdot mH_2O$ was dropped at a rate of 0.6 mL min^{-1} into 100 mL of a 0.025–0.075 M $(NH_4)_2CuCl_4\cdot 2H_2O$ solution in a flask at 290 K under argon atmosphere while stirring at a rate of 900 rpm. The pH was adjusted to 8 by adding 1.0 M NaOH (~40 mL total), after which the mixture was continuously stirred at the same rate at 290 K for 2 h. The pH was maintained at 8 by adding 1.0 M NaOH (~1 mL total). Then, the temperature of the mixture was raised to 353 K and stirred continuously for an additional 22 h, during which time the pH of the solution remained at 8. The precipitates that were obtained were filtered using a polytetrafluoroethene based membrane filter (Omnipore JGWP04700, Millipore) with a pore size of 0.2 μm and washed well with deionized water. The slurry of the precipitates was maintained under an Ar atmosphere until the end of washing. The precipitates that were obtained were dried in ambient air at 290 K for 5 days.

During the catalyst synthesis, the $[CuCl_4]^{2-}$ ions were hydrolyzed in the alkaline solution to form $[Cu(OH)_4]^{2-}$ ions (see Section 3.1). The LDH compound obtained using 0.025 M $(NH_4)_2CuCl_4\cdot 2H_2O$ solution is $[Zn_3Ga(OH)_8]^+_2[Cu(OH)_4]^{2-}\cdot mH_2O$ and abbreviated as $Zn_3Ga|Cu(OH)_4$. When 0.075 M $(NH_4)_2CuCl_4\cdot 2H_2O$ solution was used, the molar quantity of $[CuCl_4]^{2-}$ had increased by three times to form $Zn_3Ga|Cu(OH)_4$. The compound that was obtained is denoted as $[Zn_3Ga(OH)_8]^+_2[Cu(OH)_4]^{2-}\cdot mH_2O$-*3 × ex* and abbreviated as $Zn_3Ga|Cu(OH)_4$-*3 × ex*.

Cu atoms were substituted at the Zn^{II} sites of cationic layers and were also intercalated as hydroxy anions following a similar procedure to obtain $[Zn_{1.5}Cu_{1.5}Ga(OH)_8]^+$ LDH consisting of anionic Cu species. In order to set the molar ratio of Zn^{II}, Cu^{II}, and Ga^{III} ions to 3:3:2, a mixed acid solution (20 mL) was prepared as 0.375 M $Zn(NO_3)_2\cdot 6H_2O$, 0.375 M $Cu(NO_3)_2\cdot 3H_2O$, and 0.25 M $Ga(NO_3)_3\cdot nH_2O$. The 20 mL solution was dropped at a rate of 0.6 mL min^{-1} into 100 mL of a 0.025–0.075 M $(NH_4)_2CuCl_4\cdot 2H_2O$ solution in a flask at a temperature of 290 K and under an Ar atmosphere while stirring at a rate of 900 rpm. The subsequent steps in the procedure were identical to those for $Zn_3Ga|Cu(OH)_4$. The stoichiometric product starting from 0.025 M of $(NH_4)_2CuCl_4\cdot 2H_2O$ is $[Zn_{1.5}Cu_{1.5}Ga(OH)_8]^+_2[Cu(OH)_4]^{2-}\cdot mH_2O$ and abbreviated as $Zn_{1.5}Cu_{1.5}Ga|Cu(OH)_4$. In the case where three times the quantity of $(NH_4)_2CuCl_4\cdot 2H_2O$ (0.075 M) was used, the compound that was obtained is denoted as $[Zn_{1.5}Cu_{1.5}Ga(OH)_8]^+_2[Cu(OH)_4]^{2-}\cdot mH_2O$-*3 × ex* and abbreviated as $Zn_{1.5}Cu_{1.5}Ga|Cu(OH)_4$-*3 × ex*.

2.2. Characterization

Nitrogen adsorption isotherm measurements were performed at 77 K within the pressure range 1–90 kPa in a vacuum system that was connected to diffusion and rotary pumps (10^{-6} Pa) and equipped with a capacitance manometer (Models CCMT-1000A and GM-2001, ULVAC). The Brunauer–Emmett–Teller (BET) surface area (S_{BET}) was calculated on the basis of the eight-point measurements between 10 and 46 kPa (P/P_0 = 0.10–0.45) in the adsorption isotherm. As-synthesized samples were evacuated at 383 K for 2 h or at 423 K for 1 h before the measurements were taken.

X-ray diffraction (XRD) data were obtained using a MiniFlex diffractometer (Rigaku) at a Bragg angle of $2\theta_B$ = 5–70° with a scan step of 0.01° and a scan rate of 7 s per step for the sample powders. The measurements were performed at 30 kV and 15 mA using Cu Kα emission and a nickel filter.

Optical spectroscopic measurements were performed using a UV–visible spectrophotometer (JASCO, Model V-650). D_2 and halogen lamps were used for wavelengths below and above 340 nm, respectively, and an integrating sphere (JASCO, Model ISV-469) was used for the diffuse reflectance measurements. Measurements were performed at 290 K for wavelengths in the range 200–900 nm using 100 mg of fresh samples. Diffuse reflectance spectra were converted to absorption spectra on the basis of the Kubelka–Munk function [11,12]. The bandgap (E_g) value was evaluated on the basis of either simple extrapolation of the absorption edge or the fit to the Davis–Mott equation [12], given by

$$\alpha \times h\nu \propto (h\nu - E_g)^n$$

where α, h, and ν are the absorption coefficient, Planck's constant, and wavenumber, respectively, and n is 1/2, 3/2, 2, and 3 for allowed direct, forbidden direct, allowed indirect, and forbidden indirect transitions, respectively.

Cu K-edge X-ray absorption fine structure (XAFS) spectra were measured at 290 K in transmission mode in the Photon Factory at the High Energy Accelerator Research Organization on the beamlines of 9C or 7C. The storage-ring energy was 2.5 GeV, and the top-up ring current was 450 mA. A Si(1 1 1) double-crystal monochromator was inserted into the path of the X-ray beam. The X-ray intensity was maintained at 65% of the maximum flux using a piezo translator to suppress higher harmonics. The size of the slit opening in front of the I_0 ionization chamber was 1 mm (vertical) × 2 mm (horizontal). The I_0 and $I_{transmit}$ ionization chambers were purged with N_2 and Ar gases, respectively. The data accumulation time was 1 s for each data point. The Cu K absorption edge energy value was calibrated to 8980.3 eV for the spectrum of Cu metal [13,14]. The energy position of the monochromator was reproduced with an error of ±0.1 eV.

The XAFS data were analyzed using an X-ray absorption spectroscopy data analysis programme (XDAP) package [15]. The pre-edge background was approximated by a modified Victoreen function $C_2/E^2 + C_1/E + C_0$. The background of the post-edge oscillation was approximated by a smoothing spline function and calculated by an equation for the number of data points, where k is the wavenumber of photoelectrons.

$$\sum_{i=1}^{\text{Data\_Points}} \frac{(\mu x_i - BG_i)^2}{\exp(-0.075k_i{}^2)} \leq \text{smoothing factor}$$

2.3. Photocatalytic conversion tests for CO_2

As-synthesized and preheated samples of LDHs were tested for the photocatalytic conversion of CO_2 [6]. The tests were conducted in a closed circulating system (186 mL) equipped with a photoreaction quartz cell that had a flat bottom (23.8 cm^2) [16]. 100 mg

of the LDH catalyst was uniformly spread in the photoreaction cell and was evacuated by rotary and diffusion pumps (10^{-6} Pa) at 290 K for 2 h until the desorbed gas was detected by an online gas chromatograph (GC).

Reaction tests were also performed for samples of $Zn_3Ga|CO_3$ and $Zn_{1.5}Cu_{1.5}Ga|CO_3$ preheated at 423 K. The LDH sample was evacuated at 290 K and the temperature was elevated to 423 K at a rate of 4 K min^{-1}. The sample was kept at 423 K for 1 h, cooled, and transferred to the photoreaction cell using an argon filled box to prevent contact with air.

2.3 kPa of CO_2 (0.177 mmol) and 21.7 kPa of H_2 (1.67 mmol) were introduced to both intact and pretreated LDH photocatalysts and were allowed to circulate for 30 min in contact with the catalyst to attain sorption equilibrium before illumination. The photocatalyst was then illuminated with UV–visible light from the 500-W xenon arc lamp (Ushio, Model UI-502Q) from downward through the flat bottom of the quartz reactor for 5 h. The distance between the bottom of the reactor and the lamp house exit window was set to 20 mm. The light intensity at a wavelength of 555 nm was 110 mW cm^{-2} at the center of the sample cell and 73 mW cm^{-2} at the periphery of the bottom plate of the sample cell. The intensity was measured at 555 nm, but the Xe arc lamp irradiated in a wide spectrum between 200 and 1100 nm. The temperature was within the range 305–313 K at the catalyst position during the illumination for 5 h [6]. The durability test for 20 h was also performed for the $Zn_{1.5}Cu_{1.5}Ga|Cu(OH)_4$ photocatalyst.

Products and reactants were analyzed using packed columns of molecular sieve 13X-S and polyethylene glycol (PEG-6000) supported on Flusin P (GL Sciences) set in the online GC equipped with a thermal conductivity detector (Shimadzu, Model GC-8A).

3. Results

3.1. Nitrogen adsorption, XRD, UV–visible spectra, and Cu K-edge EXAFS

The S_{BET} values were measured by the N_2 adsorption at 77 K for LDH compounds treated at 383 K in a vacuum (Table 1). The S_{BET} value for $Zn_3Ga|CO_3$ was 23% greater than that for $Zn_{1.5}Cu_{1.5}Ga|CO_3$. On increasing the preheating temperature to 423 K for these LDHs, S_{BET} values increased by 18–19% (67–83 m^2 g^{-1}) due to the partial desorption of interlayer water and carbonate ions.

When compared with the S_{BET} value for $Zn_3Ga|CO_3$, the values for $Zn_3Ga|Cu(OH)_4$ and $Zn_3Ga|Cu(OH)_4$-*3* × *ex* decreased by 50–53% because of the substitution of carbonate ions with $[Cu(OH)_4]^{2-}$ ions. On the other hand, when compared with the S_{BET} value for $Zn_{1.5}Cu_{1.5}Ga|CO_3$, the values for $Zn_{1.5}Cu_{1.5}Ga|Cu(OH)_4$ and $Zn_{1.5}Cu_{1.5}Ga|Cu(OH)_4$-*3* × *ex* did not change significantly (±8.8%). The contribution of impurity phase(s) (see Section 3.1) may not be negligible.

The XRD spectra measured for as-synthesized LDH samples are shown in Fig. 1. The diffraction peaks exhibited typical patterns due to the diffraction of layer planes showing intense and sharp peaks at $2\theta_B$ = 10–35°, and also showing weak and broad peaks at $2\theta_B$ values greater than 35° [17]. There was a downward shift in several peaks at $2\theta_B$ = 11.7–11.8°, 23.5°, 34.3°, 36.9–37.0°, 38.9°, 43.6–43.7°, 46.4°, 52.6°, 56.0°, 59.4°, 60.8°, and 64.8° for $Zn_3Ga|CO_3$ (spectrum a) and $Zn_{1.5}Cu_{1.5}Ga|CO_3$ (spectrum d) by 0.4–1.5° to 11.2–11.4°, 22.5–22.7°, 33.9–34.1°, 36.4–36.5°, 38.2–38.6°, 43.1–43.2°, 45.3–45.5°, 51.1–51.4°, 54.5°, 59.0–59.2°, 60.3–60.5°, and 64.0–64.1° for $Zn_3Ga|Cu(OH)_4$ (spectrum b), $Zn_{1.5}Cu_{1.5}Ga|Cu(OH)_4$ (e), and their *3* × *ex* analogues (c and f) that were assigned to (0 0 3), (0 0 6), (0 0 9), (1 0 4), (0 1 5), (1 0 7), (0 1 8), (1 0 10), (0 1 11), (1 1 0), (1 1 3), and (1 1 6) diffractions, respectively [18,19].

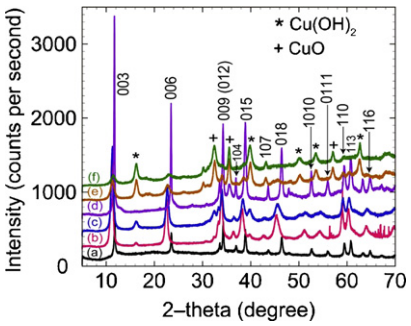

Fig. 1. XRD spectra of as-synthesized samples of $Zn_3Ga|CO_3$ (a), $Zn_3Ga|Cu(OH)_4$ (b), $Zn_3Ga|Cu(OH)_4$-*3* × *ex* (c), $Zn_{1.5}Cu_{1.5}Ga|CO_3$ (d), $Zn_{1.5}Cu_{1.5}Ga|Cu(OH)_4$ (e), and $Zn_{1.5}Cu_{1.5}Ga|Cu(OH)_4$-*3* × *ex* (f). (*) and (+) marks indicate peaks derived from $Cu(OH)_2$ and CuO powders, respectively.

In addition to characteristic LDH diffraction patterns, peaks derived from the CuO impurity phase appeared at $2\theta_B$ = 32.4–32.5°, 35.5°, and 57.0–57.1° [20,21] in the spectra of $Zn_{1.5}Cu_{1.5}Ga|Cu(OH)_4$ and the *3* × *ex* analogue (Fig. 1e and f). Peaks derived from the $Cu(OH)_2$ impurity phase appeared at $2\theta_B$ = 16.2–16.3°, 39.4°, 50.1–50.2°, 53.5–53.6°, and 62.6–62.7° [22,23] for $Zn_3Ga|Cu(OH)_4$-*3* × *ex*, $Zn_{1.5}Cu_{1.5}Ga|Cu(OH)_4$, and $Zn_{1.5}Cu_{1.5}Ga|Cu(OH)_4$-*3* × *ex* (spectra c, e, and f). The low index diffraction peaks derived from CuO or $Cu(OH)_2$ were detectable for $Zn_3Ga|Cu(OH)_4$ (b), which suggested a limited population of impurity phase(s). Diffraction peaks due to CuO and $Cu(OH)_2$ were not found for $Zn_{1.5}Cu_{1.5}Ga|CO_3$ (d).

The interlayer interval was evaluated as 0.751 and 0.753 nm on the basis of the (0 0 3) diffraction angle for $Zn_3Ga|CO_3$ and $Zn_{1.5}Cu_{1.5}Ga|CO_3$ (Table 1A and B) [24]. The values were nearly consistent with the values of 0.756 and 0.758 nm, which were evaluated based on the (0 0 6) diffraction angle. The interlayer interval values on the basis of the (0 0 9) diffraction were 0.784 and 0.785 nm. The overlap of (0 1 2) peaks on (0 0 9) peaks may be the reason for the discrepancy (0.032–0.033 nm), when compared with the corresponding values based on (0 0 3) diffraction.

On the basis of the (0 0 3) diffraction angle (Table 1A, C, and E), the interlayer interval increased from 0.751 nm for $Zn_3Ga|CO_3$ to 0.792–0.784 nm for $Zn_3Ga|Cu(OH)_4$ and $Zn_3Ga|Cu(OH)_4$-*3* × *ex*. This reflected the greater size of $[Cu(OH)_4]^{2-}$ ions when compared to that of $(CO_3)^{2-}$ [25,26]. In a similar manner, by substituting $(CO_3)^{2-}$ with $[Cu(OH)_4]^{2-}$ (Table 1B, D, and F), the interlayer interval increased from 0.753 nm for $Zn_{1.5}Cu_{1.5}Ga|CO_3$ to 0.782–0.772 nm.

The *in-plane* (1 1 0) diffraction angle (0.155–0.156 nm, Table 1) within a layer corresponds to *R*(Zn–O) of 0.219 nm if the complete ZnO_6 octahedra are assumed and remained unchanged for all of the LDH samples. In this study, the value did not change for the Zn-based LDHs [24].

The UV–visible absorption spectra for synthsized LDH compounds are depicted in Fig. 2. The E_g values were estimated by extrapolation of the absorption edge to the *x*-axis. For $Zn_3Ga|CO_3$, the intersection with the *x*-axis was at 222 nm (spectrum a), which corresponded to an E_g value of 5.6 eV (Table 1A). The E_g values were also estimated based on the fit to the Davis–Mott equation, and they were similar to 5.6 eV when *n* was 1/2 or 3/2 (Table 1A), suggesting direct electronic transition from oxygen 2p to 4s or 4p levels of Zn and Ga.

When the interlayer $(CO_3)^{2-}$ ions were replaced with $[Cu(OH)_4]^{2-}$, the UV absorption edge shifted by 60–75 nm towards the lower energy side (Fig. 2a and b). The absorption edge was extrapolated to 297 nm, corresponding to the E_g value of 4.2 eV (Table 1C). In addition, a shoulder peak near the base that extended

Table 1
Physicochemical characterization of $[Zn_{3-x}Cu_xGa(OH)_8]^+_2[A]^{2-}\cdot mH_2O$ ($x = 0$, 1.5; A = CO_3, $Cu(OH)_4$) layered double hydroxides.

Entry	Sample	S_{BET} ($m^2\,g^{-1}$)	E_g (eV)						
			Extrapolated	Fit to $\alpha \times h\nu \propto (h\nu - E_g)^n$				Interlattice Distance (nm)	
				$n = \frac{1}{2}$	$\frac{3}{2}$	2	3	(003)	(110)
A	$[Zn_3Ga(OH)_8]^+_2(CO_3)^{2-}\cdot mH_2O$ ($Zn_3Ga\|CO_3$)	70[a] (83[b])	5.6	5.9	5.4	5.2	5.0	0.751	0.155
B	$[Zn_{1.5}Cu_{1.5}Ga(OH)_8]^+_2(CO_3)^{2-}\cdot mH_2O$ ($Zn_{1.5}Cu_{1.5}Ga\|CO_3$)	57[a] (67[b])	3.5	4.2	3.2	3.0	2.6	0.753	0.155
C	$[Zn_3Ga(OH)_8]^+_2[Cu(OH)_4]^{2-}\cdot mH_2O$ ($Zn_3Ga\|Cu(OH)_4$)	35[a]	4.2	4.8	3.6	3.4	2.7	0.792	0.156
	(impurity phase(s))		3.2	4.6	3.0	2.8	2.5		
D	$[Zn_{1.5}Cu_{1.5}Ga(OH)_8]^+_2[Cu(OH)_4]^{2-}\cdot mH_2O$	62[a]	3.0	3.2	2.8	2.7	2.6	0.782	0.156
	($Zn_{1.5}Cu_{1.5}Ga\|Cu(OH)_4$)								
E	$[Zn_3Ga(OH)_8]^+_2[Cu(OH)_4]^{2-}\cdot mH_2O$-$3\times ex$	33[a]	3.6	4.2	3.1	2.8	2.6	0.784	0.156
	($Zn_3Ga\|Cu(OH)_4$-$3\times ex$)								
	(impurity phase(s))		3.1	4.1	2.9	2.6	2.0		
F	$[Zn_{1.5}Cu_{1.5}Ga(OH)_8]^+_2[Cu(OH)_4]^{2-}\cdot mH_2O$-$3\times ex$	52[a]	3.0	3.2	2.9	2.7	2.7	0.772	0.155
	($Zn_{1.5}Cu_{1.5}Ga\|Cu(OH)_4$-$3\times ex$)								

[a,b] Preheated at 383 K for 2 h[a] or 423 K for 1 h[b] under vacuum.

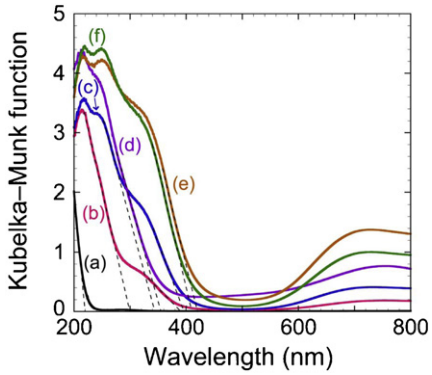

Fig. 2. Diffuse reflectance UV–visible absorption spectra of as synthesized samples of $Zn_3Ga|CO_3$ (a), $Zn_3Ga|Cu(OH)_4$ (b), $Zn_3Ga|Cu(OH)_4$-$3\times ex$ (c), $Zn_{1.5}Cu_{1.5}Ga|CO_3$ (d), $Zn_{1.5}Cu_{1.5}Ga|Cu(OH)_4$ (e), and $Zn_{1.5}Cu_{1.5}Ga|Cu(OH)_4$-$3\times ex$ (f).

close to the visible light region (Fig. 2b) was extrapolated to 390 nm (E_g = 3.2 eV). The absorption edge further shifted by 40–50 nm towards the lower energy side for $Zn_3Ga|Cu(OH)_4$-$3\times ex$ compared to that for $Zn_3Ga|Cu(OH)_4$ (spectra b→c). The absorption edge was extraporated to 348 nm (E_g = 3.6 eV; Table 1E). For spectrum c, the edge overlapped with the larger shoulder peak between 300 and 430 nm. The extrapolation of the larger shoulder resulted in an estimated E_g value of 3.1 eV (397 nm) (Table 1E).

The fits to the Davis–Mott equation resulted in similar E_g values of 4.2 and 3.6 eV, which were based on simple extrapolation (Fig. 2b and c), for $Zn_3Ga|Cu(OH)_4$ and $Zn_3Ga|Cu(OH)_4$-$3\times ex$, respectively, when n was 1/2 or 3/2 (Table 1C and E), suggesting direct electronic transition from oxygen 2p to Cu 3d, 4s, or 4p levels and Zn/Ga 4s or 4p levels.

The shoulder corresponded to E_g values of 3.1–3.2 eV for $Zn_3Ga|Cu(OH)_4$, and the $3\times ex$ analogue appeared to originate from the $Cu(OH)_2$ and/or CuO impurity phase(s) in light of the XRD spectra (Fig. 1b and c). The E_g values estimated by the fit to the Davis–Mott equation were very similar to the values that were based on simple extrapolation when n was 3/2 (Table 1C and E). This demonstrates the forbidden direct electronic transition from oxygen 2p to Cu 3d, 4s, or 4p levels of $Cu(OH)_2$ and/or CuO phase(s).

On inclusion of Cu ions in the cationic layers of $Zn_3Ga|CO_3$, the UV absorption edge shifted towards the lower energy side for $Zn_{1.5}Cu_{1.5}Ga|CO_3$ (Fig. 2d) when compared to the corresponding LDH free from Cu (spectrum a). Simple extrapolation yielded an E_g value of 3.5 eV (354 nm; Table 1B). Upon further replacing interlayer $(CO_3)^{2-}$ ions with $[Cu(OH)_4]^{2-}$ ions, the UV absorption edge shifted by 65–75 nm towards the lower energy side (Fig. 2e).

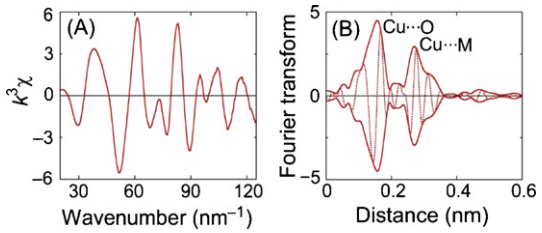

Fig. 3. Cu K-edge EXAFS spectra for $Zn_3Ga|Cu(OH)_4$-$3\times ex$ sample. (A) k^3-weighted EXAFS χ-function and (B) its associated Fourier transform. The solid and dotted lines represent the magnitude and the imaginary part in (B).

Simple extrapolation of the absorption edge resulted in an intersection with the x-axis at 417 nm (E_g = 3.0 eV; Table 1D).

The absorption edge for the LDH sample for which three times the amount of $[CuCl_4]^{2-}$ was used for the synthesis (Fig. 2f) was extrapolated to 407 nm (E_g = 3.0 eV, Table 1F). For the case of n ranging from 1/2 or 3/2, the fits of the spectrum to the Davis–Mott equation resulted in very similar estimates of the E_g values based on simple extrapolation for $Zn_{1.5}Cu_{1.5}Ga|Cu(OH)_4$ and $Zn_{1.5}Cu_{1.5}Ga|Cu(OH)_4$-$3\times ex$ (Table 1D and F).

In summary, the E_g value (5.6 eV) for $Zn_3Ga|CO_3$ that is free from copper decreased to 4.2 and 3.5 eV on the inclusion of Cu between and within layers, respectively, and decreased further to 3.0 eV on the inclusion of Cu at both locations. The electronic transition was considered to be directly from O 2p to metal (n–1)d, ns, or np. In addition, the forbidden direct electronic transition (3.1–3.2 eV) from oxygen 2p to Cu 3d, 4s, or 4p levels of $Cu(OH)_2$ and/or CuO impurity phase(s) was observed.

The Cu K-edge EXAFS spectrum was tentatively measured for the $Zn_3Ga|Cu(OH)_4$-$3\times ex$ sample (Fig. 3). In the Fourier transform (panel B), two intense peaks appeared at 0.16 and 0.27 nm (phase shift uncorrected). The peak that was derived from Cu–Cl bond(s) would appear at 0.195 nm [27] (phase shift uncorrected; true bond distances 0.2270–0.2287 nm) [28,29], but no peak appeared at the distance in Fig. 3B. Therefore, no Cu–Cl peaks were found in the Fourier transform for this LDH photocatalyst (Fig. 3B), demonstrating the complete hydrolysis of $[CuCl_4]^{2-}$ into $[Cu(OH)_4]^{2-}$.

3.2. Photocatalytic conversion of CO_2

While $Zn_3Ga|CO_3$ was CO selective (80 nmol h^{-1} $g_{cat}{}^{-1}$) in 2.3 kPa of CO_2 and 21.7 kPa of H_2 under the illumination of UV–visible light (Fig. 4A and Table 2A), $Zn_{1.5}Cu_{1.5}Ga|CO_3$ was methanol selective (170 nmol h^{-1} $g_{cat}{}^{-1}$ and 68 mol%; Fig. 4B and Table 2B).

Table 2
Rates of photocatalytic conversion of CO_2 with H_2 into CH_3OH and CO over LDH photocatalysts.[a]

Entry	Photocatalyst	Formation rate (nmol h^{-1} g_{cat}^{-1})			Conversion (%, C-base)	Selectivity to CH_3OH (mol%)
		CH_3OH	CO	Σ		
A	$Zn_3Ga|CO_3$	51(±4)	80(±6)	130	0.02	39(±4)
B	$Zn_{1.5}Cu_{1.5}Ga|CO_3$	170(±14)	79(±6)	250	0.03	68(±4)
C	$Zn_3Ga|CO_3$[b]	50(±4)	74(±6)	120	0.02	40(±4)
D	$Zn_{1.5}Cu_{1.5}Ga|CO_3$[b]	310(±9)	180(±2)	500	0.07	63(±1)
E	$Zn_3Ga|Cu(OH)_4$	300(±9)	130(±10)	430	0.04	71(±2)
F	$Zn_{1.5}Cu_{1.5}Ga|Cu(OH)_4$	490(±15)	70(±6)	560	0.05	88(±2)
G	$Zn_3Ga|Cu(OH)_4$-3×*ex*	280(±8)	120(±9)	390	0.04	71(±3)
H	$Zn_{1.5}Cu_{1.5}Ga|Cu(OH)_4$-3×*ex*	430(±13)	48(±4)	480	0.05	90(±1)

[a] The catalyst amount was 100 mg. Values in the parentheses are experimental errors for evaluation.
[b] Preheated at 423 K for 1 h under vacuum.

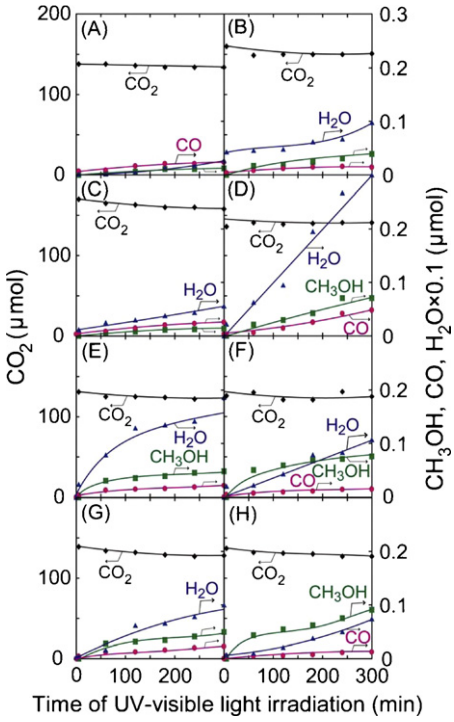

Fig. 4. Time course of photocatalytic reactions in CO_2 (2.3 kPa) + H_2 (21.7 kPa). Hundred milligram of the LDH catalyst was charged: fresh $Zn_3Ga|CO_3$ (A), $Zn_{1.5}Cu_{1.5}Ga|CO_3$ (B), $Zn_3Ga|CO_3$ preheated at 423 K (C), $Zn_{1.5}Cu_{1.5}Ga|CO_3$ preheated at 423 K (D), fresh $Zn_3Ga|Cu(OH)_4$ (E), $Zn_{1.5}Cu_{1.5}Ga|Cu(OH)_4$ (F), $Zn_3Ga|Cu(OH)_4$-3 × *ex* (G), and $Zn_{1.5}Cu_{1.5}Ga|Cu(OH)_4$-3 × *ex* (H). The reactor was illuminated from a 500-W Xe arc lamp. CO_2 (♦; diamond), H_2O (▲; triangle), CH_3OH (■; square), and CO (●; circle).

When the $Zn_3Ga|CO_3$ sample was preheated at 423 K in a vacuum, the change in the photocatalytic performance was negligible (Fig. 4C and A). In contrast, when $Zn_{1.5}Cu_{1.5}Ga|CO_3$ was preheated at 423 K (Fig. 4D), the methanol formation rate increased by a factor of 1.8 (310 nmol h^{-1} g_{cat}^{-1}; Table 2D and B). The availability of interlayer sites bound to Cu was considered to be critical for CO_2 photoreduction.

The $Zn_3Ga|Cu(OH)_4$ photocatalyst was then tested (Fig. 4E). The methanol formation rate was enhanced by a factor of 5.9 compared to that using $Zn_3Ga|CO_3$ (Table 2E and A). The methanol selectivity was nearly the same as that obtained using $Zn_{1.5}Cu_{1.5}Ga|CO_3$ (71–68 mol%). Cu sites between interlayers and within cationic layers may work similarly in photocatalysis. On the other hand, the interlayer Cu sites boosted the methanol formation rates by a factor of 5.9 as opposed to the promotion of Cu sites in $[Zn_{1.5}Cu_{1.5}Ga(OH)_8]^+$ layers, which boosted the methanol formation rates by a factor of 3.3 (Table 2E, B and A).

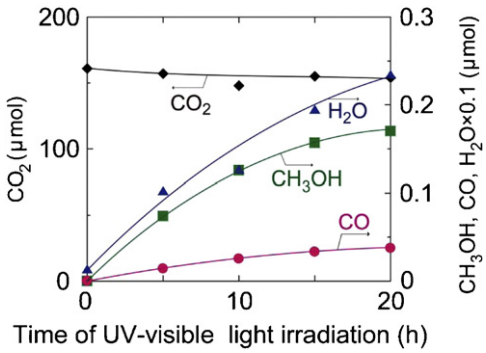

Fig. 5. Time course of photoreactions in CO_2 (2.3 kPa) + H_2 (21.7 kPa) using 100 mg of $Zn_{1.5}Cu_{1.5}Ga|Cu(OH)_4$ for 20 h. Other reaction conditions and legends are the same as those for Fig. 4.

Using $Zn_{1.5}Cu_{1.5}Ga|Cu(OH)_4$ (Fig. 4F), the methanol formation rate and selectivity were further improved to 490 nmol h^{-1} g_{cat}^{-1} and 88 mol% (Table 2F) owing to the combination of Cu sites within layers and Cu sites between layers.

In addition, photocatalysis using $Zn_3Ga|Cu(OH)_4$-3 × *ex* was compared with an exact stoichiometric $Zn_3Ga|Cu(OH)_4$ sample to evaluate the effects of Cu impurities. The decrease in the product formation rates was only 5.6–8.6% (Table 2E and G). The catalytic effects of Cu impurities were greater for $Zn_{1.5}Cu_{1.5}Ga|Cu(OH)_4$-3 × *ex* compared to its stoichiometric analogue (12–31%; Table 2H and F). However, the effect was still relatively small.

In the kinetic tests (Fig. 4), the formation rates of water were between 0.3 and 3.0 μmol h^{-1} g_{cat}^{-1}. These rates exceeded the quantity of water that was catalytically formed as the products of the following equations:

$$CO_2 + H_2 \rightarrow CO + H_2O$$

$$CO_2 + 3H_2 \rightarrow CH_3OH + H_2O$$

This discrepancy is due to the desorption of interlayer water molecules of LDHs [30,31].

Finally, the durability of the $Zn_{1.5}Cu_{1.5}Ga|Cu(OH)_4$ photocatalyst (100 mg) was tested for 20 h in CO_2 (2.3 kPa) + H_2 (21.7 kPa) illuminated with UV–visible light from the 500-W xenon arc lamp. In the test, methanol formation continued and the selectivity was 76–84 mol% (Fig. 5). After every 5 h, the methanol formation rate gradually decreased from 145 to 101, 61, and subsequently to 26 nmol h^{-1} g_{cat}^{-1}, while the CO formation rate decreased from 28 to 23, 15 and finally 8.2 nmol h^{-1} g_{cat}^{-1}. Throughout the test, the only products that were identified were methanol, CO, and water.

Table 3
Rates of photocatalytic formation of CH_3OH and CO per specific surface area and the quantity of Cu in the LDH photocatalysts.[a]

Entry	Photocatalyst	Formation rate per specific surface area ($nmol\,h^{-1}\,m^{-2}$)			Formation rate per amount of Cu ($nmol\,h^{-1}\,mmol_{Cu}{}^{-1}$)		
		CH_3OH	CO	Σ	CH_3OH	CO	Σ
A	$Zn_3Ga\|CO_3$	0.73	1.1	1.9	–	–	–
B	$Zn_{1.5}Cu_{1.5}Ga\|CO_3$	3.0	1.4	4.4	51	24	77
C	$Zn_3Ga\|CO_3$[b]	0.60	0.89	1.5	–	–	–
D	$Zn_{1.5}Cu_{1.5}Ga\|CO_3$[b]	4.7	2.7	7.4	97	56	150
E	$Zn_3Ga\|Cu(OH)_4$	8.6	3.6	12	300	130	430
F	$Zn_{1.5}Cu_{1.5}Ga\|Cu(OH)_4$	7.9	1.1	9.1	120	17	140

[a] The catalyst amount was 100 mg. Values in the parentheses are experimental errors for evaluation.
[b] Preheated at 423 K for 1 h under vacuum.

4. Discussion

4.1. Improvement in photocatalysis by preheating of LDH photocatalysts

The layered structure of the synthesized compounds of the formula for $[Zn_{3-x}Cu_xGa(OH)_8]^+{}_2(CO_3)^{2-}\cdot mH_2O$ was confirmed by XRD. The interlayer distance of these compounds ranged from 0.751 to 0.753 nm, and the S_{BET} values ranged from 57 to 70 $m^2\,g^{-1}$. The E_g value of $Zn_3Ga|CO_3$ was 5.6 eV. Upon the addition of Cu sites in the layers to form $Zn_{1.5}Cu_{1.5}Ga|CO_3$, the E_g value decreased to 3.5 eV.

Heating these samples under vacuum conditions at 423 K resulted in the removal of one third of the water and interlayer carbonate ions [6], while the S_{BET} value increased by 18–19%. The S_{BET} increase for $Zn_{1.5}Cu_{1.5}Ga|CO_3$ does not adequately explain the increase of the methanol and CO formation rates by a factor of 1.8 and 2.3, respectively (Table 2D). The layered structure and the composition of the cationic layer did not change based on the XRD and UV–visible absorption pattern (Figs. 1 and 2). The available interlayer space that was created at 423 K is expected to facilitate the diffusion of CO_2 into the reaction space and the reaction with the surface hydroxy groups that are bound to the Cu sites (the Graphical abstract).

4.2. Role of in-layer and interlayer Cu in photocatalysis

Based on the tentative Cu K-edge EXAFS data, no chlorine coordination was observed for the $Zn_3Ga|Cu(OH)_4$-$3\times ex$ sample. Therefore, during catalyst synthesis, the following reactions (at least partially) took place.

$$[CuCl_4]^{2-} + 4NaOH \rightarrow [Cu(OH)_4]^{2-} + 4NaCl \quad (1)$$

$$2[Zn_3Ga(OH)_8]^+ + [Cu(OH)_4]^{2-} + mH_2O \rightleftarrows [Zn_3Ga(OH)_8]_2^+ [Cu(OH)_4]^{2-}\cdot mH_2O \quad (2)$$

$$[Zn_3Ga(OH)_8]_2^+[Cu(OH)_4]^{2-}\cdot mH_2O \rightleftarrows Zn_6Ga_2(OH)_{15}\{(\mu-O)Cu(OH)_3\}\cdot mH_2O + H_2O \quad (3)$$

$$Zn_6Ga_2(OH)_{15}\{(\mu-O)Cu(OH)_3\}\cdot mH_2O \rightleftarrows Zn_6Ga_2(OH)_{14}\{(\mu-O)_2Cu(OH)_2\}\cdot mH_2O + H_2O \quad (4)$$

$$Zn_6Ga_2(OH)_{14}\{(\mu-O)_2Cu(OH)_2\}\cdot mH_2O \rightleftarrows Zn_6Ga_2(OH)_{13}\{(\mu-O)_3Cu(OH)\}\cdot mH_2O + H_2O \quad (5)$$

By substituting $(CO_3)^{2-}$ anions for $[Cu(OH)_4]^{2-}$ ions, the S_{BET} values decreased by 50–53% for $[Zn_3Ga(OH)_8]^+$ LDHs, and did not change significantly for $[Zn_{1.5}Cu_{1.5}Ga(OH)_8]^+$ LDHs (Table 1). The formation rates per specific catalyst surface area and the formation rates for specific quantities of Cu are summarized in Table 3. The methanol formation rates per specific surface area were greater for Cu containing LDHs, especially those which consisted of $[Cu(OH)_4]^{2-}$, whereas there was no significant variation in the CO formation rates per specific surface area. For the $Zn_{1.5}Cu_{1.5}Ga|CO_3$ photocatalyst, the formation rates of methanol and CO were 51 and 24 $nmol\,h^{-1}\,mmol_{Cu}{}^{-1}$, respectively. These values increased to 97 and 56 $nmol\,h^{-1}\,mmol_{Cu}{}^{-1}$, respectively, when heated at 423 K in a vacuum. For the $Zn_3Ga|Cu(OH)_4$ photocatalyst, the formation rates of methanol and CO were 300 and 130 $nmol\,h^{-1}\,mmol_{Cu}{}^{-1}$, respectively. Therefore, the interlayer Cu sites were 5.3–5.9 times more effective than Cu sites in cationic layers, if we assume that the Cu atoms are primary active sites.

The methanol formation rate per unit amount of photocatalyst was optimum when using $Zn_{1.5}Cu_{1.5}Ga|Cu(OH)_4$ that consisted of both in-layer and interlayer Cu sites (Table 2F). The methanol formation rate per unit amount of Cu was 120 $nmol\,h^{-1}\,mmol_{Cu}{}^{-1}$ (Table 3F), which is in close agreement with the calculated value of 110 $nmol\,h^{-1}\,mmol_{Cu}{}^{-1}$, which was contributed by the in-layer Cu sites ($3/4\times 51$ $nmol\,h^{-1}\,mmol_{Cu}{}^{-1}$) and the interlayer Cu sites ($1/4\times 300$ $nmol\,h^{-1}\,mmol_{Cu}{}^{-1}$).

During the synthesis of LDH $3\times ex$ analogues, one third (2.5 mmol) of the $(NH_4)_2CuCl_4\cdot 2H_2O$ compound was used to produce 2.5 mmol of LDHs (2.50–2.51 g). Two thirds (5.0 mmol) of the $(NH_4)_2CuCl_4\cdot 2H_2O$ would produce 0.40–0.48 g of CuO & $Cu(OH)_2$, depending on the population ratio. Therefore, the contents of Cu impurity phases are 14–16 wt% in $Zn_3Ga|Cu(OH)_4$-$3\times ex$ and $Zn_{1.5}Cu_{1.5}Ga|Cu(OH)_4$-$3\times ex$, which are in good agreement with the photocatalytic rate decrease of 5.6–8.6% and 12–31%, respectively (Table 2). The Cu impurity phases appear to be inactive.

The introduction of Cu in the interlayer space of LDHs accomplished two purposes. First, it resulted in an increase in the interlayer distance from 0.751 nm for $Zn_3Ga|CO_3$ to 0.792 nm for $Zn_3Ga|Cu(OH)_4$, in effect expanding the interlayer reaction space. A similar change was observed for $[Zn_{1.5}Cu_{1.5}Ga(OH)_8]^+$ layers where the increase was from 0.753 nm for carbonate containing LDH to 0.782 nm for $[Cu(OH)_4]^{2-}$ containing LDH. Secondly, the introduction of Cu resulted in the transformation to semiconductors as demonstrated by the decrease of the E_g values to 3.0–4.2 eV (Table 1). The UV–visible absorption edge shifted towards the lower energy side and dramatically increased the excitation energy region for the photocatalysis.

It is interesting to compare the catalytic performance between interlayer Cu hydroxy anions and Cu octahedral sites surrounded by six oxygen atoms in the LDH cationic layers. Although the doped quantity of Cu was one third for the former sites, the methanol formation rates increased by a factor of 5.9 due to the replacement of

carbonates with $[Cu(OH)_4]^{2-}$ anions, as opposed to the increase by a factor of 3.3 due to the replacement of Zn sites with Cu (Table 2). The steric availability (accessibility) of $[Cu(OH)_4]^{2-}$ may be related to the reactivity difference (the Graphical abstract), but the exact speciation of doped Cu hydroxy groups (as in Eqs. (1)–(5)) is required for detailed discussion.

In this study, hydrogen was used to achieve CO_2 photoreduction, but we also demonstrated the feasibility of using LDH photocatalysts and water to achieve CO_2 photoreduction. 2.6 kPa of CO_2 was applied to 7 mg of $Zn_{1.5}Cu_{1.5}Ga|CO_3$ and subsequently converted to methanol at a rate of 5.1 μmol h^{-1} $g_{cat}{}^{-1}$ and coupled with hydrogen species activated from water using 20 mg of Pt/C catalyst separated by a proton conducting polymer film. Currently, heating at 413 K is required to make the polymer proton-conductive. Also, the totally photocatalytic photoreduction of CO_2 using water is being researched.

5. Conclusions

The photoreduction of CO_2 into methanol with hydrogen using $[Zn_{1.5}Cu_{1.5}Ga(OH)_8]^+{}_2(CO_3)^{2-}{\cdot}mH_2O$ was improved by a factor of 1.8 by preheating at 423 K in a vacuum. The available interlayer space was created at 423 K and is expected to facilitate the diffusion of CO_2 to the reaction space and the reaction with the surface hydroxy groups that are bound to Cu sites.

By substituting the $(CO_3)^{2-}$ for $[Cu(OH)_4]^{2-}$, the methanol formation rates using $[Zn_3Ga(OH)_8]^+{}_2(CO_3)^{2-}{\cdot}mH_2O$ and $[Zn_{1.5}Cu_{1.5}Ga(OH)_8]^+{}_2(CO_3)^{2-}{\cdot}mH_2O$ increased by a factor of 5.9 and 2.9, respectively. The hydroxy groups that were bound to Cu sites were important, and the effects of the interlayer $[Cu(OH)_4]^{2-}$ were greater than those of the in-layer octahedral Cu sites because of its steric availability (accessibility) and semiconductivity (E_g values of 3.0–4.2 eV).

Acknowledgements

The authors are thankful for financial supports received from the Grant-in-Aid for Scientific Research C (2255 0117) from the Ministry of Education, Culture, Sports, Science and Technology (MEXT) (2010–2011) and received from the Asahi Glass Foundation (2009–2010). The X-ray absorption experiments were performed with the approval of the Photon Factory Proposal Review Committee (No. 2009G552). The authors thank Prof. Yoshitake for providing the Xe arc lamp and Prof. Kaneko and Prof. Kanoh for the XRD apparatus.

References

[1] C. Song, Catal. Today 115 (2006) 2.
[2] C.D. Ferguson, Nature 471 (2011) 411.
[3] I.H. Tseng, W.C. Chang, J.C.S. Wu, Appl. Catal. B 37 (2002) 37.
[4] Q. Liu, Y. Zhou, J. Kou, X. Chen, Z. Tian, J. Gao, S. Yan, Z. Zou, J. Am. Chem. Soc. 132 (2010) 14385.
[5] K. Koci, V. Matejka, P. Kovar, Z. Lacny, L. Obalova, Catal. Today 161 (2011) 105.
[6] N. Ahmed, Y. Shibata, T. Taniguchi, Y. Izumi, J. Catal. 279 (2011) 123.
[7] G.K. Mor, K. Shankar, M. Paulose, O.K. Varghese, C.A. Grimes, Nano Lett. 5 (2005) 191.
[8] Z. Ding, H.Y. Zhu, P.F. Greenfield, G.Q. Lu, J. Colloid Interface Sci. 238 (2001) 267.
[9] D.G. Costa, A.B. Rocha, W.F. Souza, S.S.X. Chiaro, A.A. Leitao, J. Phys. Chem. B 115 (2011) 3531.
[10] S.K. Yun, T.J. Pinnavaia, Chem. Mater 7 (1995) 348.
[11] Y. Izumi, T. Itoi, S. Peng, K. Oka, Y. Shibata, J. Phys. Chem. C 113 (2009) 6706.
[12] X. Gao, I.E. Wachs, J. Phys. Chem. B 104 (2000) 1261.
[13] J.A. Bearden, Rev. Mod. Phys. 39 (1967) 78.
[14] G. Zschornack, Handbook of X-ray Data, Springer, Berlin/Heidelberg, 2007, p. 233.
[15] M. Vaarkamp, H. Linders, D. Koningsberger, XDAP version 2.2.7 (2006), XAFS Services International, Woudenberg, The Netherlands.
[16] Y. Izumi, K. Konishi, H. Yoshitake, Bull. Chem. Soc. Jpn. 81 (2008) 1241.
[17] E. Coronado, C. Marti-Gastaldo, E. Navarro-Moratalla, A. Ribera, Appl. Clay Sci. 48 (2010) 228.
[18] Y. Sun, Y. Zhou, Z. Wang, X. Ye, Appl. Surf. Sci. 255 (2009) 6372.
[19] A. Ennadi, A. Legrouri, A. De Roy, J.P. Besse, J. Solid State Chem. 152 (2000) 568.
[20] H. Wu, X. Wei, M. Shao, J. Gu, M. Qu, Chem. Phys. Lett. 364 (2002) 152.
[21] J. Pike, S. Chan, F. Zhang, X. Wang, J. Hanson, Appl. Catal. A 303 (2006) 273.
[22] W. Zhang, X. Wen, S. Yang, Y. Berta, Z.L. Wang, Adv. Mater. 15 (2003) 822.
[23] X. Wu, H. Bai, J. Zhang, F. Chen, G. Shi, J. Phys. Chem. B 109 (2005) 22836.
[24] F. Cavani, F. Trifiro, A. Vaccari, Catal. Today 11 (1991) 173.
[25] G.W. Brindley, S. Kikkawa, Clays Clay Minerals 28 (1980) 87.
[26] D. Yan, J. Lu, J. Ma, M. Wei, S. Qin, L. Chen, D.G. Evans, X. Duan, J. Mater. Chem. 20 (2010) 5016.
[27] G. Leofanti, M. Padovan, M. Garilli, D. Carmello, A. Zecchina, G. Spoto, S. Bordiga, G. Turnes Palomino, C. Lamberti, J. Catal. 189 (2000) 91.
[28] J.A. McGinnety, J. Am. Chem. Soc. 94 (1972) 8406.
[29] G. Li, D.M. Camaioni, J.E. Amonette, Z.C. Zhang, T.J. Johnson, J.L. Fulton, J. Phys. Chem. B 114 (2010) 12614.
[30] P.J. Sideris, U.G. Nielsen, Z. Gan, C.P. Grey, Science 321 (2008) 113.
[31] J.T. Klogregge, L. Hickey, R.L. Frost, J. Solid State Chem. 177 (2004) 4047.